High-Performance Hydraulic Soft Robotic Control Using Continuous Flow Regulation and Partial Feedback

Shijian Wu, Kailuan Tang, *Graduate Student Member, IEEE*, Shaowu Tang, *Graduate Student Member, IEEE*, Sicong Liu, *Member, IEEE*, Juan Yi, Jian Sheng Dai, *Fellow, IEEE*, and Zheng Wang, *Senior Member, IEEE*

***Abstract*—Hydraulic-driven soft robots have received much less attention than their pneumatic counterparts. However, the incompressibility of liquid could bring a series of desirable attributes to soft robotic control, despite the apparent disadvantage of weight addition and compliance compromise resulting from the liquid medium itself, as well as the performance limitations of the hydraulic pump and valve systems being used. In this article, we introduce a Hydraulic Actuation with Wide-range Flow regulation (HAWF) as the fundamental inner control loop, and propose a soft robotic hydraulic control framework with Characteristics-based Control and Partial State feedback (CCPS), exploiting the desirable features of flow-regulating devices such as peristaltic pumps, achieving accurate and fast-responding position/force regulation on different soft actuators. The proposed control framework is validated with different control devices for comparisons, with promising results. The proposed framework could be generalizable to other hydraulic-driven systems towards control performance and simplified system setup across different applications.**

***Index Terms*—Flow regulation, hydraulic actuation, position/force regulation, soft robotics.**

I. Introduction

SOFT robots, characterized by their soft material bodies and the resulting high degrees of freedom, have emerged as promising candidates in various scenarios, such as human-robot interactions and manipulation of delicate objects. Their high adaptability and safety compared to the rigid ones [1], [2] in complex environments make them particularly well-suited for these applications [3], [4], [5], [6], [7]. Close-loop control is essential for soft robots to perform effectively in diverse situations and environments. However, the intrinsic properties of soft materials and actuation methods, including low elastic modulus, nonlinearity, hysteresis, and viscoelastic effects, pose challenges to the implementation of closed-loop control. [8], [9], [10].

Apart from perception where numerous solutions have been proposed [9], [10], [11], [12], [13], actuation is another decisive factor for accurate closed-loop control of soft robots. Specific implementations vary notably with the actuation type. Therefore, to progress soft robotics and enhance performance across diverse applications, it is significant to comprehend and explore various actuation methods. Among actuating approaches of soft robots such as pneumatic actuation [14], dielectric actuation [15], and magnetic actuation [16], hydraulic actuation is the one implemented by pressurizing and depressurizing liquid in designated cavities inside soft robots to induce expected motion/force. The incompressibility of the liquid endows hydraulic soft robots with both positive and negative attributes. Despite disadvantages including lower compliance pneumatic ones, performance reduction once being punctured, and difficult miniaturization, hydraulic soft robots exhibit attractive advantages including high stability, high load capacity, high actuating force, high response frequency, and various motion patterns such as bending, elongating, and twisting [3], [5], [6], [17].

In recent years, various hydraulic actuation methods have been applied to soft robots. Pump & valve systems with switch control, are based on discrete operations (on/off) of their components. These systems are prevalent in implements of actuation of fluidic-driven soft robots for their high design adaptability and versatility to a wide range of robotic applications [18], [19], [20], [21], [22]. However, even if their speeds are high, the discrete flow controlled with on/off valves leads to challenges of accurate control such as oscillations [19], [21], [23]. Additionally, there is a contradiction between response time and regulation precision for hydraulic systems controlling on/off valves. This contraction could be overcome by applying a proper algorithm on parallelly-connected high-speed valves but at the expense of cost, weight, and complexity [23], [24], [25], [26].

Alternatively, research efforts have focused on actuation methods allowing bidirectional continuous flow regulation,

Manuscript received 12 January 2024; accepted 26 May 2024. Date of publication 19 June 2024; date of current version 26 June 2024. This letter was recommended for publication by Associate Editor S. Song and Editor Y.-L. Park upon evaluation of the reviewers' comments. This work was supported in part by NSFC under Grant 52105021, and in part by Shenzhen Science, Tech. and Innovation Commission under Grant ZDSYS20220527171403009 and Grant RCBS20210609104446099. *(Corresponding authors: Juan Yi; Zheng Wang.)*

Shijian Wu, Juan Yi, and Jian Sheng Dai are with the Shenzhen Key Laboratory of Intelligent Robotics and Flexible Manufacturing Systems, Southern University of Science and Technology, Shenzhen 518055, China, and also with the Department of Mechanical and Energy Engineering, Southern University of Science and Technology, Shenzhen 518055, China (e-mail: 12132305@mail.sustech.edu.cn; yij3@sustech.edu.cn).

Kailuan Tang is with the School of Mechatronics Engineering, Harbin Institute of Technology, Harbin 150001, China, and also with the Department of Mechanical and Energy Engineering, Southern University of Science and Technology, Shenzhen 518055, China (e-mail: tangkl@mail.sustech.edu.cn).

Shaowu Tang, Sicong Liu, and Zheng Wang are with the Department of Mechanical and Energy Engineering, Southern University of Science and Technology, Shenzhen 518055, China (e-mail: zheng.wang@ieee.org).

This letter has supplementary downloadable material available at https://doi.org/10.1109/LRA.2024.3416770, provided by the authors.

Digital Object Identifier 10.1109/LRA.2024.3416770

including cylinder & piston systems and peristaltic pumps. Capable of transferring liquid precisely, cylinder & piston systems are suitable for scenarios where high precision is emphasized instead of fast response, such as characterizing a novel actuator [27], or actuating soft robots that carry another device requiring accurate pose control [28], [29], [30]. Peristaltic pumps independently enable valveless, bidirectional liquid transferring without backflow, and consequently untethered designs in a compact form factor [31], and even open-loop positional control with mapping between the motor position and the actuator motion in a specific motor speed interval [32], [33]. With a model based on air compressibility, the flow-regulating capability of peristaltic pumps was proven effective in closed-loop pneumatic pressure control, which enables rapid and stable soft robotic position control indirectly [34]. Hence, the flow regulation capability of peristaltic pumps remains worthwhile to investigate to hold promising prospects for further advancing the overall control performance of soft robotics for various applications.

In this study, we further explore the potential of utilizing the flow regulation method in terms of wide-range flow rates for close-loop control of soft hydraulic robotic systems. The model determined by soft robots in control is employed for fast and accurate position and force control compared to the prevalent pump & valve systems. The main contributions of this work are as follows:

- Proposing a concept of Hydraulic Actuation with Wide-range Flow Regulation (HAWF), which refers to regulating the rate of a continuous flow in a wide range in terms of both its direction and magnitude to actuate soft hydraulic robots, thus enabling soft robots to converge quickly and steadily.
- Presenting a Characteristics-based Control with Partial State-feedback (CCPS) method to cooperate with the HAWF concept for soft hydraulic actuators. Based on partial state feedback (i.e. output feedback), flow regulation is guided by a model based on the physical and task-related characteristics of the actuator, contributing to high accuracy, dynamic performance, and adaptability.
- Constructing an embodiment system with a peristaltic pump for flow regulating device since it fulfills the needs of the HAWF method with a compact form factor. Experiments are conducted for thorough verification, including comparisons with conventional pump & valve systems.

The remaining part of this letter comprises the HAWF concept and design of our hydraulic actuation system (Section II), CCPS method and design of controllers (Section III), platform setup descriptions and experimental procedures for validation (Section IV), the experimental results and discussions (Section V), and the conclusions and future work (Section VI).

II. HAWF Concept and Design of Hydraulic Actuation System

A. HAWF Concept

In a simplified circuit driving an actuator with a peristaltic pump (see Fig. 1(a)), as the peristaltic pump is propelled, water is transferred. The direction of transferring determines whether

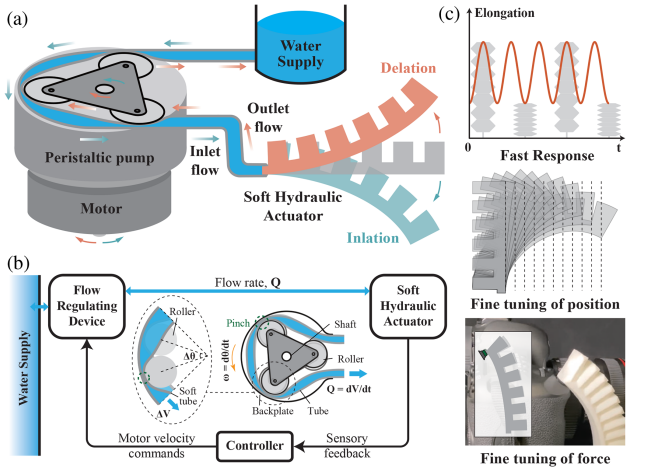

Fig. 1. Concept of HAWF method and design of hydraulic actuation system. (a) Simplified system driving an actuator with a peristaltic pump. (b) Hydraulic actuation system based on flow regulation with a peristaltic pump. (c) Characteristics of the proposed hydraulic actuation system.

the actuator inflates or deflates. As is shown in Fig. 1(b), when the shaft is driven by a motor to rotate through $\Delta\theta$, a volume ΔV of liquid will be squeezed out or taken in, depending on the direction of $\Delta\theta$, which means the ability of bidirectional transferring. Besides bidirectional transferring, backflow could be prevented because the tube is constantly pinched regardless of the motor velocity. Based on bidirectional transferring and backflow prevention, the flow rate $Q = dV/dt$ could be regulated continuously by controlling the motor velocity $\omega = d\theta/dt$ in a wide range in terms of both its direction and magnitude. Thus, quick converging and oscillation avoidance can be compatible while actuating soft robots with a regulated continuous flow.

McIntyre et al. [35] proposed and validated a model for solving the average flow rate of peristaltic pumps with constant motor velocity ($\leq$5 rev/s) and end-to-end pressure difference:

$$Q_{avg} = \frac{(V_{nom} - V_r \cdot NU)\omega}{2\pi} \tag{1}$$

where Q_{avg} is the average flow rate of the pump, V_{nom} is the nominal volume displacement of the pump determined by the pump dimensions, V_r is the maximum roller volume displacement value measured experimentally, NU is the number of rollers, and ω is the motor velocity. The first three parameters in (1) are all constants concurrently influenced by factors including the circuit configuration, the number of rollers, pump dimensions, and the pressure difference across the pump, therefore, the flow rate of a peristaltic pump is proportional to the motor velocity in a steady state.

However, it is difficult to predict the flow rate of a peristaltic pump accurately and dynamically in real-time scenarios since the motor velocity and end-to-end pressure difference may change over time. As a consequence, close-loop control is crucial for the robustness of control.

B. Design of Hydraulic Actuation System

For better adaptability and accurate control of soft hydraulic actuators, a hydraulic actuation system was constructed for

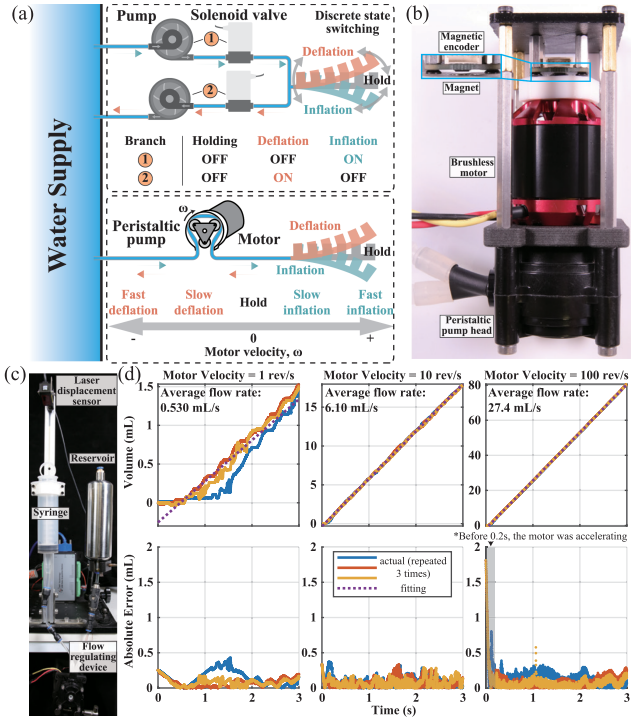

Fig. 2. Pump & valve system and flow regulating device. (a) Comparison between a pump & valve system and a flow regulating device. (b) Components of the flow regulating device (ODrive excluded). (c) Experimental setup measuring the transferred volume of the flow regulating device. (d) First row: transferred volume of the flow regulating device vs. time with motor velocities of distinct degrees of magnitude (plotted with solid lines) and linearly fitting curve(plotted with dashed lines); second row: absolute error between the original curve and the fitting one vs. time. (In every graph, three solid lines with distinct colors represent results of repeated experiments.).

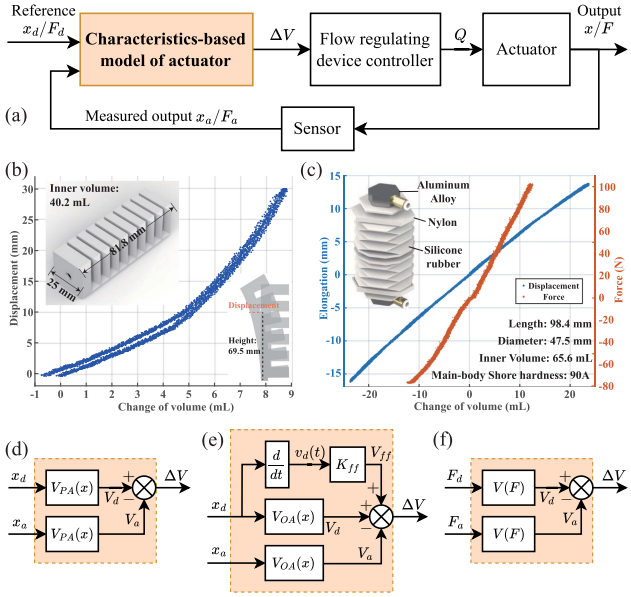

Fig. 3. CCPS method and design of controllers. (a) Diagrams of CCPS method. (b) PneuNet actuator for experiments and the relationship between its displacement at a fixed height and change of its volume. (c) Origami actuator for experiments and the relationships between its elongation/output force and change of its volume. Physicality-based model for (d) Position control of a PneuNet actuator. (e) Position control of an origami actuator. (f) Force control of actuators.

closed-loop control as depicted in Fig. 1(b): as per the sensory feedback of the actuator, the controller sends commands to the flow regulating device to adjust the motor velocity, so that the flow rate into the actuator will be regulated to reduce the error.

There are co-existing characteristics of the proposed hydraulic actuation system based on the HAWF method (see Fig. 1(c)): Not only can the flow rate be large with a high motor speed so that the actuator can respond fast, but fine-tuning of position/force can be supported with the motor rotating slowly, enabling dexterous operations such as imitating a human finger to shoot a picture with a camera.

1) Design of Flow Regulating Device: Fig. 2(a) depicts how a flow regulating device differs from a pump & valve system while actuating a hybrid-pressure hydraulic actuator. For a pump & valve system, two branches are utilized to inflate and deflate the actuator respectively. The system can be switched to three discrete operation states, but it is difficult to regulate the flow rate directly, and transitions are not instant, which makes overshooting and oscillations possible due to the incompressibility of liquid. By comparison, the flow rate through a peristaltic pump can be regulated continuously with the motor velocity so that the motion state of the actuator changes smoothly.

To implement our system, the controller runs on a computer, receiving sensory data from a data acquisition device and sending motor velocity commands to the flow regulating device. As is shown in Fig. 2(b), the flow regulating device consists of a peristaltic pump head, a 560 KV brushless motor, a magnetic encoder, and a magnet fixed on the shaft of the motor controlled with an open-source field-oriented control device enabling precise velocity control.

2) Verification for HAWF: To prove the reliability and repeatability of the flow regulating device, a preliminary test was conducted on the setup shown in Fig. 2(c), where the flow regulating device pumped water from a reservoir into a syringe with the motor velocity of 1, 10, and 100 rev/s in triplicate, respectively. The displacement of the syringe piston was measured with a laser displacement sensor to calculate the transferred volume over time. The results were shown in Fig. 2(d), which indicated that with distinct steady-state motor velocities, the errors between the original curve and the fitting one are of the same degree of magnitude. It can be observed that when the motor velocity increased by a factor of 10 from 1 rev/s, the average flow rate increased to 11.5 times the original values, which is in accordance with (1), and when the motor velocity further increased by a factor of 10, (1) failed to hold since the average flow rate merely increased to 4.49 times the original values, which could be attributed to cavitation.

III. CCPS Method and Design of Controllers

A. CCPS Method

Although the constructed hydraulic actuation system has shown its reliable flow regulation capability, it is necessary to design the controller properly faced with various actuators and tasks. To tackle this problem, as is shown in Fig. 3(a), the CCPS method centers a model mainly based on the physical characteristics of actuators, and requires feedback on the output

(e.g. position or force) of the system solely to produce a volume increment. Then the volume increment is input to the flow regulating device controller (a PD controller) to regulate the flow rate accordingly. For further clarification, in the following sections, position control and force control of two distinct actuators will be implemented and validated experimentally. The sensory feedback for our system and pump & valve systems was provided by off-shelf sensors so that the potential of the HAWF concept and CCPS method on soft robotic control can be better validated and compared.

B. Design of Controllers

1) Position Control of an PneuNet Actuator: A PneuNet actuator inspired by [36] had been printed with thermoplastic polyurethane (TPU) and utilized in this work. Its dimensions and relationship between displacement at a fixed height and change of volume can be found in Fig. 3(b), where the nonlinearity could be observed (coefficient of determination $R^2 = 0.928$). The position control of this actuator is supposed to adapt the nonlinearity of the displacement-volume relationship and converge successfully. As a consequence, the volume estimation function $V_{PA}(x)$ in the characteristics-based model (see Fig. 3(d)) is obtained by polynomial fitting and then applied to calculate the volume increment ΔV.

2) Position Control of an Origami Actuator: The relationship between elongation and change of volume, and the basic parameters of the origami actuator we designed were shown in Fig. 3(c), and more details are available in our previous works [22], [37]. Besides the physical characteristics of the actuator, the demands of the task could be a crucial factor for the design of the characteristics-based model. The objective of its position control is tracking a given position trajectory accurately, requiring high dynamic performance. Therefore, the characteristics-based model design for this actuator is depicted in Fig. 3(e). The actuator has a linear elongation-volume relationship (coefficient of determination $R^2 = 0.998$), leading to a linear function $V_{OA}(x)$ for volume estimation. To enhance the dynamic performance, a feed-forward item, i.e., a multiple of the currently desired actuator velocity, is added with the volume difference to obtain the volume increment ΔV.

3) Force Control of Actuators: For the origami actuator fixed in the initial position, as is shown in Fig. 3(c), the force-volume relationship is also linear (coefficient of determination $R^2 = 0.992$), but the volume range is much narrower than that of elongation. For the PneuNet actuator, the force control will be validated in a camera operating experiment, where short travel and mild force are expected while pressing and releasing the shutter button. Therefore, in the model for force control, the volume difference estimation function $V(F)$ in the model (see Fig. 3(f)) is linear, and the feedforward item can be omitted.

IV. Soft Robotic Control Platform Setup and Validation

Fig. 4(a) interprets briefly how experiments of position control and force control were conducted on the origami actuator. In experiments of position control, the actuator was fixed on one end and driven to elongate axially, and the displacement was measured by a displacement sensor. Moreover, a load was involved as a variable for robustness assessment.

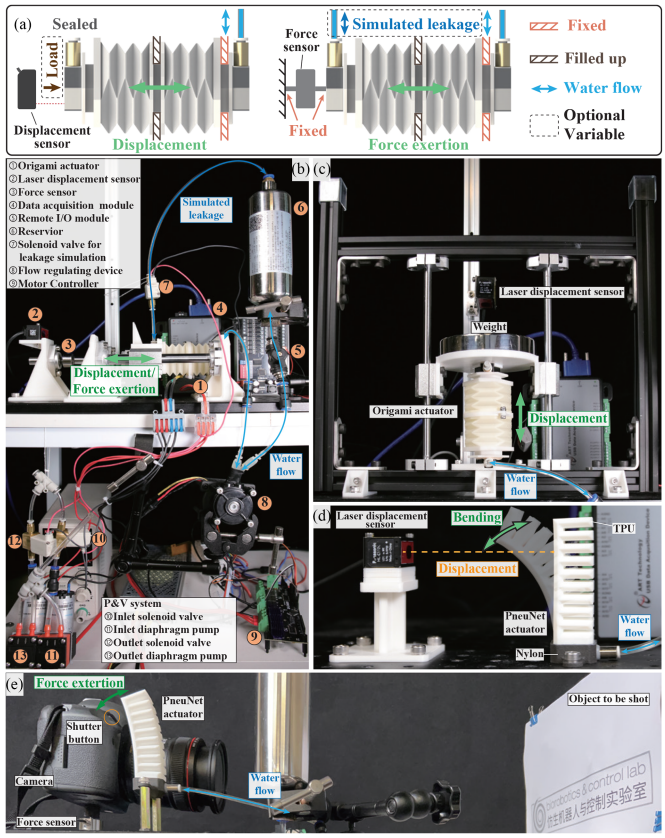

Fig. 4. Actuators and experimental setups. (a) Diagrams of experiments of position control and force control. (b) The experimental setup for position control tests (without load) and force control tests, and the pump and valve system. (c) The experimental setup for the position control tests (with load). (d) The experimental setup for the demonstration of position control of a PneuNet actuator. (e) The experimental setup for the demonstration of force control of a PneuNet actuator.

In experiments of force control, both ends of the actuator were fixed and one was fixed across a force sensor measuring the force exerted by the driven actuator. In addition, leakage simulated with a solenoid valve was introduced as a variable for robustness assessment. Although it was pointed out that leakage could hinder the performance of actuators [3], [5], [6], it remained worthwhile to verify whether this disturbance could be compensated properly with the HAWF capability and CCPS method of our system or not with sufficient liquid supply. The actuator's neck was filled up to avoid unexpected inflation. In each test, the desired curve and the actual one would be recorded to calculate the root-mean-square error (RMSE).

A. Position Control Experiments for an Origami Actuator

The experimental setup for position control experiments is shown in Fig. 4(b)(c). In Fig. 4(b), an origami actuator was constrained with a linear guide fixed horizontally to ensure its free axial elongation while a laser displacement sensor measured the elongation. In Fig. 4(c), both the linear guide and the actuator

were installed vertically so that weights on the tray could exert load on the actuator.

1) Test with a Trapezoidal Velocity Trajectory: Trapezoidal velocity trajectory is a position control strategy commonly applied to motors. Given a target position, a trapezoidal velocity trajectory, whose integral equals the displacement between the target position and the current one (depicted as an S-shaped curve over time), will be calculated for velocity control with predefined acceleration, deceleration, and maximum velocity. To exhibit that our system meets the requirements in an applicable scenario, the position control strategy mentioned above was implemented for the origami actuator and evaluated experimentally. Two tests were conducted on setups in Fig. 4(b)(c) respectively, depending on whether the actuator is loaded or not. The acceleration, deceleration, and maximum velocity of trapezoidal velocity trajectory were assigned as 5 mm/s^2, 5 mm/s^2, and 5 mm/s in both tests.

2) Frequency Response Comparison Test: To prove the advantage of our system in the accuracy and dynamic performance of position control w.r.t. pump & valve systems, a frequency response comparison test was conducted on the setup in Fig. 4(b), with a sinusoidal position curve $x(t) = A[1 - \cos(2\pi ft)]/2$ as the target of position control. Nevertheless, switch control with a deadzone of ± 0.1 mm is utilized to control pump & valve systems. To reveal how the hardware limitations impact the performance of pump & valve systems, two pump & valve systems with identical diaphragm pumps and distinct solenoid valves with a small orifice (1 mm diameter) and a large orifice (5 mm diameter) respectively, for a larger valve orifice was expected to allow a higher flow rate.

B. Force Control Experiments for an Origami Actuator

Tests for force control were performed on the setup in Fig. 4(b), where the origami actuator was constrained at its initial position with its output force measured by a force sensor, and a solenoid valve (1 mm diameter) was connected between the actuator and the reservoir for leakage simulation.

1) Step Response Comparison Test: In this test, to evaluate and compare the capability of force control, the actuator was driven by our system and pump & valve systems respectively from the initial state (zero force output) to the target force on 5 equal steps, and then driven to zero force on 5 equal steps. Every step took 1 s. And whether the leak is simulated or not is a variable as well.

2) Frequency Response Comparison Test: Similar to the frequency response comparison test for position control, a sinusoidal force curve $F(t) = A[1 - \cos(2\pi ft)]/2$ is input as the target. And as a variable, simulated leakage played a role of disturbance in the process of force control, since a minor volume loss could impair the force output. The deadzone of switch control of pump & valve systems was ± 2 N.

C. Experiments for a PneuNet Actuator

The goal of this test is to prove that with a characteristics-based model, our system could handle the nonlinearity of an actuator and succeed in controlling its position or force stably.

1) Accurate Position Control: As is shown in Fig. 4(d), a PneuNet actuator was installed vertically. A laser displacement sensor measured its displacement at a height of 69.5 mm. In this test, the actuator was driven from the initial state (0 mm) to 28 mm in a step length of 1 mm, and every step took 2 s. The process mentioned above was conducted with distinct volume estimation functions in the characteristics-based model, which were obtained by polynomial fitting with orders ranging from 1 to 3.

2) Photographing Test: Owing to high compliance, soft actuators are inherently safe while directly interacting with delicate objects like a camera. In the experimental setup shown in Fig. 4(e), a camera was installed on a force sensor, and a PneuNet actuator was installed in a proper position to make sure that it could reach the shutter button while bending.

At first, the camera was operated by hand under the procedure below: press the button mildly to focus, release to cancel focusing, press mildly again to focus, press harder to shoot, and release to finish. In this procedure, force was recorded to figure out the thresholds triggering focusing and shooting. Then the procedure was repeated with the PneuNet actuator according to known force thresholds.

V. Results of Soft Robotic Control Experiments

A. Position Control Experiments for an Origami Actuator

1) Test with a Trapezoidal Velocity Trajectory: It is shown in Fig. 5(b) that with our system, an actuator could elongate along the desired position and velocity curve, and the RMSE$<$0.2 mm of position control if -15 mm $\leq x_d \leq$ 15 mm. Additionally, Fig. 5(c) indicated that the accuracy would remain even if the actuator was under a load of less than 4.14 kg, which proved the robustness as well as the practical potential of our hydraulic actuation system.

2) Frequency Response Comparison Test: It can be observed in Fig. 6 that as the required response amplitude and frequency increased, RMSEs of two pump & valve systems noticeably increased while our system could keep the RMSE$<$1.5 mm. For example, when $A = -15$ mm, $f = 0.5$ Hz, the RMSE of our system is 67.1% lower than those of pump & valve systems at least; when $A = 15$ mm, $f = 0.5$ Hz, the RMSE of our system is 76.1% lower than those of pump & valve systems at least. To gain deeper insight, select two groups where one pump & valve system shows significantly larger RMSE than others, and compare all displacement-time curves. On the one hand, when $A = 5$ mm, $f = 0.1$ Hz, the actuation system was meant to drive the actuator to move slowly, but large orifices of valves resulted in a large flow rate and consequently a large step length for every operation of pump & valve that caused oscillations in the graph. On the other hand, when $A = 5$ mm, $f = 0.5$ Hz, the actuator was supposed to move quickly and change its direction sharply, however, the small orifice of valves restricted the maximum flow rate and thus hindered the actual position from catching up to the desired position that was changing acutely. The discussion above clarified the contradiction between response time and regulation precision in pump & valve systems. Attributed to its HAWF capability, our system could handle input of position control oscillating with distinct amplitudes and frequencies.

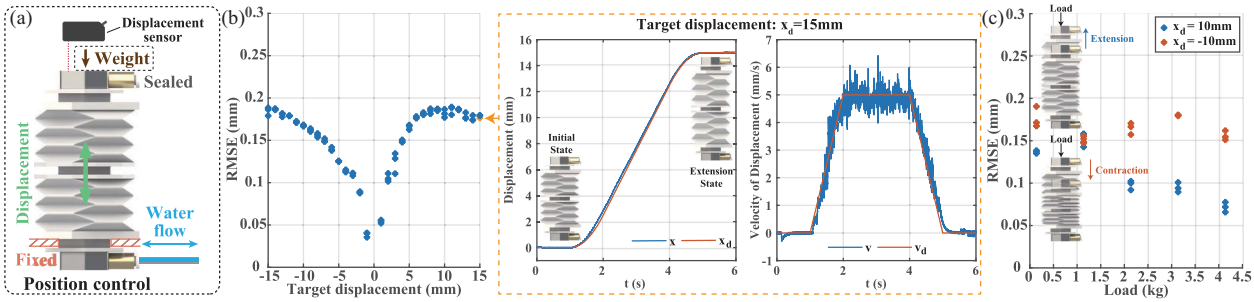

Fig. 5. Results of the position control test with a trapezoidal velocity trajectory. (a) Diagram of position control tests. (b) Left: RMSE vs. target displacement in the test for position control with a trapezoidal velocity trajectory; right: actual and desired displacement and velocity vs. time with the target displacement of 15 mm. (c) RMSE vs. load exerted on the actuator in the test for position control with a trapezoidal velocity trajectory.

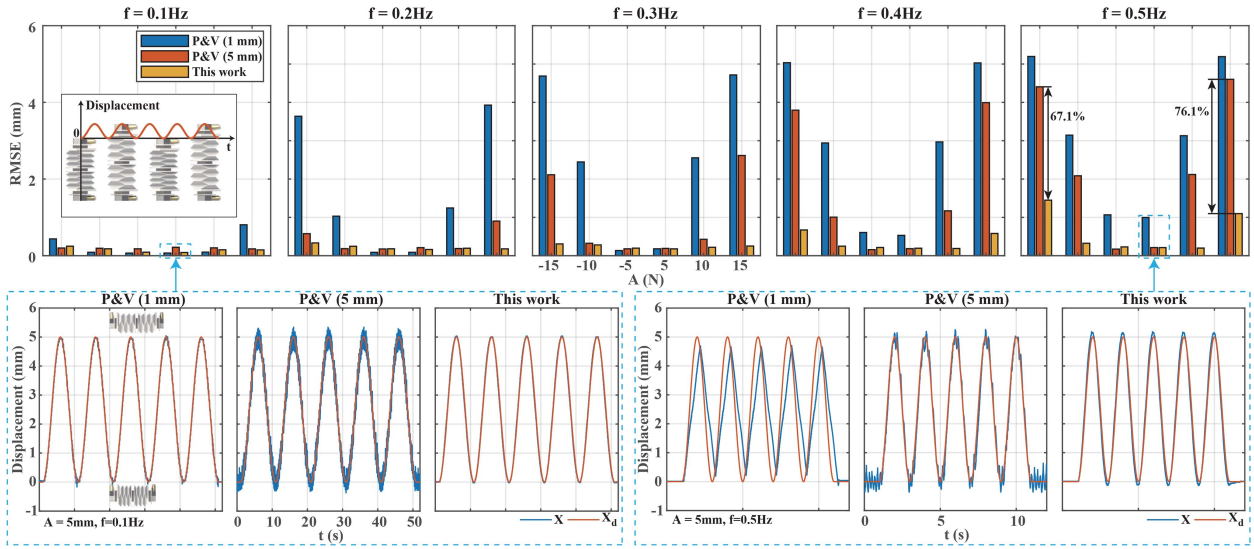

Fig. 6. Results of the frequency response comparison test of position control. First row: RMSE vs. A in the frequency response comparison test for position control; second row: comparison of actual and desired displacement vs. time with $A = 5$ mm, $f = 0.1$ Hz, and $A = 5$ mm, $f = 0.5$ Hz respectively.

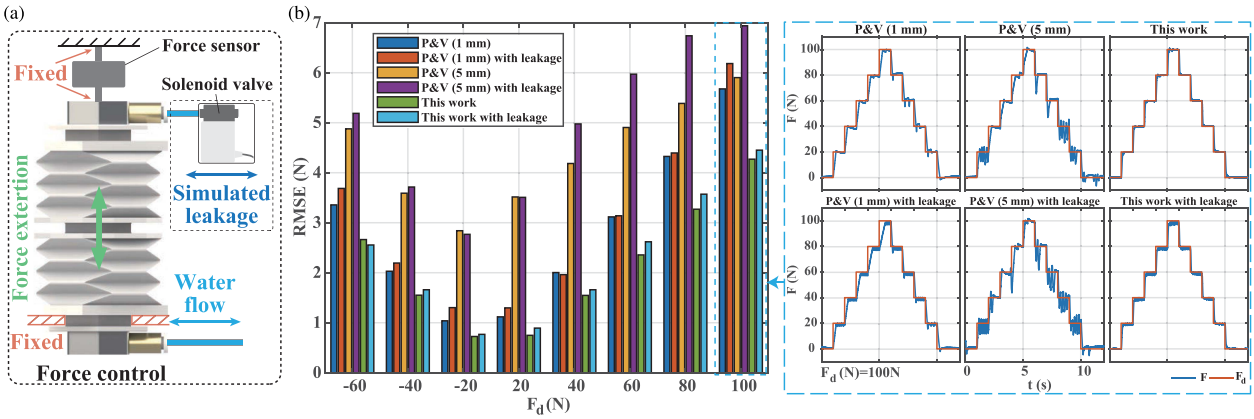

Fig. 7. Results of the step response comparison test of force control. (a) Diagram of force control tests. (b) Upper: RMSE vs. A in the step response comparison test for force control; lower: comparison of actual and desired force vs. time with the target force of 100 N.

B. Force Control Experiments for an Origami Actuator

1) Step Response Comparison Test: The RMSE vs. target force in step response comparison test for force control is shown in Fig. 7(b). It was observed that our system had the lowest RMSEs, and the simulated leakage would lead to a larger RMSE in most groups. When the target force was equal to 100 N, as more oscillations were introduced along with simulated leakage, failures to converge in 1 s became more frequent for the pump & valve system with large orifices because of its large step length.

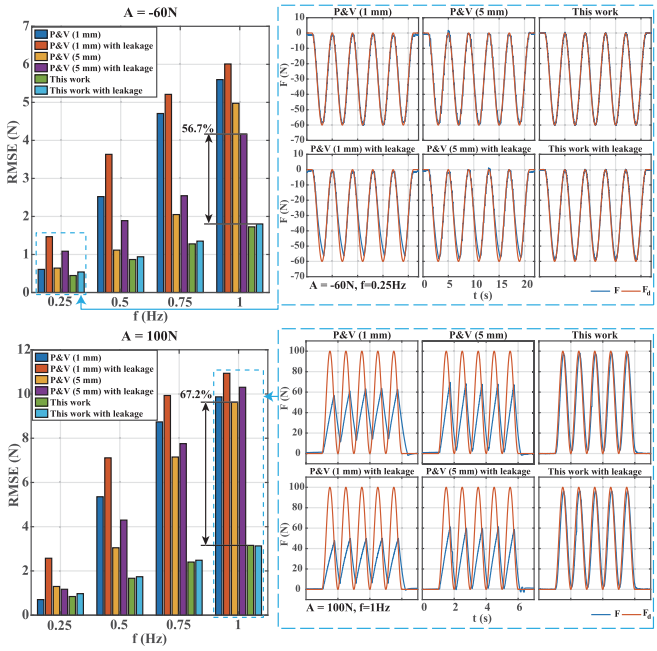

Fig. 8. Results of the frequency response comparison test of force control. First column: RMSE vs. A in the frequency response comparison test for force control with $A = -60$ N and $A = 100$ N; second column: comparison of actual and desired force vs. time with $A = -60$ N, $f = 0.25$ Hz and $A = 100$ N, $f = 1$ Hz respectively.

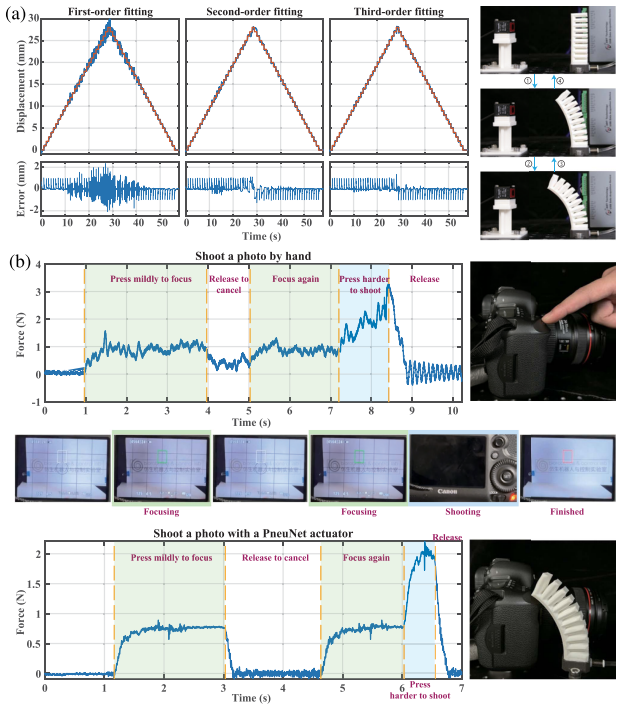

Fig. 9. Results of demonstrations of a PneuNet actuator. (a) Displacement and its error vs. time in accurate position control with different volume estimation functions in the characteristics-based model. (b) Upper: force vs. time while shooting a picture by hand; middle: procedure of operating the camera; lower: force vs. time while shooting a picture with a PneuNet actuator.

On the contrary, our system could manage to converge regardless of whether leakage was simulated or not. This distinction could be attributed to the fact that when the leakage was simulated, compensating operations of pump & valve systems happened only if the deviation of force from the target value exceeded the deadzone, but our system kept compensating even if the deviation was minor. In addition, compared to the pump & valve system with small orifices, our system could converge more rapidly with a larger flow rate at the very beginning of every step.

2) Frequency Response Comparison Test: It can be concluded from Fig. 8 that faced with an ever-changing target force, our system could obtain the highest accuracy and robustness even against disturbances among three actuation systems. For example, when $A = -60$ N, $f = 1$ Hz, the RMSE of our system is 56.7% lower than those of pump & valve systems at least; when $A = 100$ N, $f = 1$ Hz, the RMSE of our system is 67.2% lower than those of pump & valve systems at least. To figure out how the simulated leakage impacted distinct systems, select two groups dealing with targets of distinct amplitudes and frequencies. When $A = -60$ N, $f = 0.25$ Hz and leakage happened, errors of pump & valve systems increased as the force increased, which could be attributed to that higher pressure led to a higher flow rate through the open orifice of the leakage-simulating solenoid valve and the net flow rate of pump & valve systems would be inadequate. In contrast, our system could compensate for the disturbance of leakage at different pressures with its HAWF capability, which explains why RMSE did not increase as significantly as those of other systems after the leakage happened. When $A = 100$ N, $f = 1$ Hz, the insufficiency of flow rates of both pump & valve systems turned out to be the dominant factor for error, however, our system was able to actuate the actuator as desired with a higher flow rate. It was proven that apart from handling tough input targets, when the water supply can be guaranteed (e.g. actuation in the underwater environments [31]), our system could also compensate disturbances such as leakage, to which actuators are supposed to be prone. With this dynamic compensation capability, our system could be applied to a wider range of applications in soft robotics.

C. Experiments for a PneuNet Actuator

1) Accurate Position Control: Fig. 9(a) shows that as the polynomial order increased for fitting of volume estimation function, successful convergences of position control in 2 s were more and more frequent for the PneuNet actuator, which shows the effectiveness of the characteristics-based model for coping with the nonlinear behavior of an actuator.

2) Shutter-Release Test: In the beginning, through the procedure completed by hand shown in the upper part in Fig. 9(b), the threshold triggering focusing and shooting could be determined as 0.8 N and 2.0 N, respectively. Then with these known thresholds, the PneuNet actuator was able to repeat the procedure and the force-time curve was recorded in the lower part in Fig. 9(b). And it can be observed that the curve was even steadier in the lower part than its counterpart, because the physiological tremor is inevitable for humans, but actuators are not prone to this disadvantage. The process was recorded in the supplementary video.

VI. Conclusion and Future Work

In this letter, we proposed the HAWF concept and CCPS method, and implemented a hydraulic actuation system enabling fast- and fine-tuning of soft robots. The system was tested and compared to conventional pump & valve systems experimentally, on an origami actuator, and turned out to perform position/force control with higher accuracy and robustness against disturbances than its counterparts. Lastly, in the position control experiment for a PneuNet actuator, it was proven that with the CCPS method, an actuator with a nonlinear motion behavior can also be controlled accurately. In the final demonstration of camera shutter-releasing, the soft actuator with CCPS could very clearly distinguish between a shutter half-press and a shutter full-press, two states only separable by the pressing force. The combination of achievable features together with the compact form factor and the simplified hydraulic circuit setup, could potentially pave the way for some more diversified explorations and applications of hydraulic soft robots.

The prospective work may focus on, perfecting hardware and controllers to further improve performance and versatility in more complicated interactive tasks, integrating with state-of-the-art perceptive approaches of soft robots, and exploring wider applications of multi-actuator systems.

References

[1] J. A. Saglia, N. G. Tsagarakis, J. S. Dai, and D. G. Caldwell, "Control strategies for ankle rehabilitation using a high performance ankle exerciser," in *Proc. IEEE Int. Conf. Robot. Automat.*, 2010, pp. 2221–2227.

[2] F. Aimedee et al., "Systematization of morphing in reconfigurable mechanisms," *Mech. Mach. Theory*, vol. 96, pp. 215–224, Feb. 2016.

[3] O. Yasa et al., "An overview of soft robotics," *Annu. Rev. Control Robot. Auton. Syst.*, vol. 6, no. 1, pp. 1–29, 2023.

[4] M. Li et al., "Soft actuators for real-world applications," *Nature Rev. Mater.*, vol. 7, no. 3, pp. 235–249, Mar. 2022.

[5] W. Dou et al., "Soft robotic manipulators: Designs, actuation, stiffness tuning, and sensing," *Adv. Mater. Technol.*, vol. 6, no. 9, 2021, Art. no. 2100018.

[6] N. El-Atab et al., "Soft actuators for soft robotic applications: A review," *Adv. Intell. Syst.*, vol. 2, no. 10, 2020, Art. no. 2000128.

[7] X. Dong et al., "Recent advances in biomimetic soft robotics: Fabrication approaches, driven strategies and applications," *Soft Matter*, vol. 18, no. 40, pp. 7699–7734, Oct. 2022.

[8] L. Wang and F. Iida, "Deformation in soft-matter robotics: A categorization and quantitative characterization," *IEEE Robot. Automat. Mag.*, vol. 22, no. 3, pp. 125–139, Sep. 2015.

[9] H. Wang et al., "Toward perceptive soft robots: Progress and challenges," *Adv. Sci.*, vol. 5, no. 9, 2018, Art. no. 1800541.

[10] Z. Lin et al., "Recent advances in perceptive intelligence for soft robotics," *Adv. Intell. Syst.*, vol. 5, no. 5, 2023, Art. no. 2200329.

[11] L. Wang et al., "Soft robot proprioception using unified soft body encoding and recurrent neural network," *Soft Robot.*, vol. 10, no. 4, pp. 825–837, Aug. 2023.

[12] Z. Fang et al., "Multi-dimensional proprioception and stiffness tuning for soft robotic joints," in *Proc. IEEE Int. Conf. Robot. Automat.*, 2022, pp. 10973–10979.

[13] Y. Cheng et al., "A multimodal hydrogel soft-robotic sensor for multifunctional perception," *Front. Robot. AI*, vol. 8, 2021, Art. no. 692754.

[14] D. S. Shah et al., "A soft robot that adapts to environments through shape change," *Nature Mach. Intell.*, vol. 3, no. 1, pp. 51–59, Jan. 2021.

[15] G. Li et al., "Self-powered soft robot in the mariana trench," *Nature*, vol. 591, no. 7848, pp. 66–71, Mar. 2021.

[16] Y. Dong et al., "Untethered small-scale magnetic soft robot with programmable magnetization and integrated multifunctional modules," *Sci. Adv.*, vol. 8, no. 25, Jun. 2022, Art. no. eabn8932.

[17] X. Chen et al., "A review of soft manipulator research, applications, and opportunities," *J. Field Robot.*, vol. 39, no. 3, pp. 281–311, 2022.

[18] J. Wang and A. Chortos, "Control strategies for soft robot systems," *Adv. Intell. Syst.*, vol. 4, no. 5, May 2022, Art. no. 2100165.

[19] P. Polygerinos et al., "Soft robotic glove for combined assistance and at-home rehabilitation," *Robot. Auton. Syst.*, vol. 73, pp. 135–143, Nov. 2015.

[20] S. Chen et al., "A pneumatic–hydraulic hybrid actuator for underwater soft robot swimming and crawling," *Sens. Actuators A, Phys.*, vol. 356, Jun. 2023, Art. no. 114284.

[21] Z. Shen et al., "An underwater robotic manipulator with soft bladders and compact depth-independent actuation," *Soft Robot.*, vol. 7, no. 5, pp. 535–549, Oct. 2020.

[22] K. Tang et al., "A strong underwater soft manipulator with planarly-bundled actuators and accurate position control," *IEEE Robot. Automat. Lett.*, vol. 8, no. 11, pp. 7559–7566, Nov. 2023.

[23] H. Wang et al., "Development of high-speed on–off valves and their applications," *Chin. J. Mech. Eng.*, vol. 35, no. 1, Jun. 2022, Art. no. 67.

[24] Y. Shang et al., "A research of high-precision pressure regulation algorithm based on ON/OFF valves for aircraft braking system," *IEEE Trans. Ind. Electron.*, vol. 69, no. 8, pp. 7797–7806, Aug. 2022.

[25] F. Sciatti et al., "Digital hydraulic valves: Advancements in research," *Heliyon*, vol. 10, no. 5, Mar. 2024, Art. no. e27264.

[26] R. Ding et al., "Programmable hydraulic control technique in construction machinery: Status, challenges and countermeasures," *Automat. Constr.*, vol. 95, pp. 172–192, Nov. 2018.

[27] J. Peters, B. Anvari, C. Chen, Z. Lim, and H. A. Wurdemann, "Hybrid fluidic actuation for a foam-based soft actuator," in *Proc. IEEE/RSJ Int. Conf. Intell. Robots Syst.*, 2020, pp. 8701–8708.

[28] L. Lindenroth, S. Bano, A. Stilli, J. G. Manjaly, and D. Stoyanov, "A fluidic soft robot for needle guidance and motion compensation in intratympanic steroid injections," *IEEE Robot. Automat. Lett.*, vol. 6, no. 2, pp. 871–878, Apr. 2021.

[29] L. Lindenroth, R. J. Housden, S. Wang, J. Back, K. Rhode, and H. Liu, "Design and integration of a parallel, soft robotic end-effector for extracorporeal ultrasound," *IEEE Trans. Biomed. Eng.*, vol. 67, no. 8, pp. 2215–2229, Aug. 2020.

[30] R. Zhang et al., "A cephalopod-inspired soft-robotic siphon for thrust vectoring and flow rate regulation," *Soft Robot.*, vol. 8, no. 4, pp. 416–431, Aug. 2021.

[31] Q. Tan et al., "Underwater crawling robot with hydraulic soft actuators," *Front. Robot. AI*, vol. 8, 2021, Art. no. 688697.

[32] M. A. Bell et al., "A modular and self-contained fluidic engine for soft actuators," *Adv. Intell. Syst.*, vol. 4, no. 1, Jan. 2022, Art. no. 2100094.

[33] M. A. Bell et al., "An ambidextrous STarfish-Inspired exploration and reconnaissance robot (the ASTER-bot)," *Soft Robot.*, vol. 9, no. 5, pp. 991–1000, Oct. 2022.

[34] C. Hu, J. Kang, J. Liu, J. Wang, and H. Liao, "Peristaltic pump-based palm-sized multi-mode pressure supply system for soft robots," *IEEE Robot. Automat. Lett.*, vol. 9, no. 3, pp. 2120–2127, Mar. 2024.

[35] M. P. McIntyre et al., "Modelling the pulsatile flow rate and pressure response of a roller-type peristaltic pump," *Sens. Actuators A, Phys.*, vol. 325, Jul. 2021, Art. no. 112708.

[36] Y. Zhai et al., "Desktop fabrication of monolithic soft robotic devices with embedded fluidic control circuits," *Sci. Robot.*, vol. 8, no. 79, Jun. 2023, Art. no. eadg3792.

[37] S. Tang et al., "Performance enhancement of the soft robotic segment for a trunk-like arm," *Front. Robot. AI*, vol. 10, Jul. 2023, Art. no. 1210217.